crystals

MDPI

Article

Ultra-Wideband Terahertz Wave Absorber Using Vertically Structured IGIGIM Metasurface

Muhammad Asif [1], Qiong Wang [1,*], Zhengbiao Ouyang [1,*], Mi Lin [1] and Zixian Liang [2]

[1] THz Technical Research Center of Shenzhen University, Shenzhen Key Laboratory of Micro-Nano Photonic Information Technology, Key Laboratory of Optoelectronic Devices and Systems of Ministry of Education and Guangdong Province, College of Physics and Optoelectronic Engineering, Shenzhen University, Shenzhen 518060, China; rmasif@email.szu.edu.cn (M.A.)

[2] Institute of Microscale Optoelectronics, Shenzhen University, Shenzhen 518060, China; zixianliang@szu.edu.cn

* Correspondence: qwang@szu.edu.cn (Q.W.); zbouyang@szu.edu.cn (Z.O.)

Abstract: Achieving perfect absorption of electromagnetic waves across a wide range of frequencies is crucial for various applications, including sensing, imaging, and energy capture. In this study, we introduced a new concept for metasurfaces and proposed a six-layer vertically structured IGIGIM metasurface consisting of gold (Au), silicon (Si), graphene (G_1), silica (SiO_2), a second layer of graphene (G_2), and polymethyl methacrylate (PMMA), which demonstrates ultra-wideband absorptance in the terahertz (THz) region. Through theoretical analysis and numerical simulations, we obtained broadband absorptance over 80% with the average absorptance of 92.6% and a bandwidth of 8.22 THz, from 1.78 to 10.0 THz. Whereas, dual broadband absorptance was obtained for above 90% with the bandwidth of 5.63 THz in the two sub-bands of 2.09–3.5 THz and 5.78–10 THz and above 95% with the bandwidth of 3.63 THz in the two sub-bands of 2.32–3.12 THz and 6.35–9.9 THz. Moreover, the proposed structure exhibits a polarization-independent absorption property. Also, it demonstrates a tolerance for the incident angle of 40 degrees, maintaining a wide absorption band. This remarkable feature is attributed to the multiple Fabry–Pérot resonance absorptions in the structure. Our study presents a convenient method for designing high-quality terahertz wave absorbers with outstanding broadband absorptance.

Keywords: terahertz; absorber; ultra-wideband; metasurface; graphene; IGIGIM structure

check for updates

Citation: Asif, M.; Wang, Q.; Ouyang, Z.; Lin, M.; Liang, Z. Ultra-Wideband Terahertz Wave Absorber Using Vertically Structured IGIGIM Metasurface. *Crystals* **2024**, *14*, 22. https://doi.org/10.3390/cryst14010022

Academic Editors: Kerlos Atia Abdalmalak, Raed Shubair, Ayman Althuwayb and Bal S. Virdee

Received: 28 November 2023
Revised: 19 December 2023
Accepted: 21 December 2023
Published: 25 December 2023

Copyright: © 2023 by the authors. Licensee MDPI, Basel, Switzerland. This article is an open access article distributed under the terms and conditions of the Creative Commons Attribution (CC BY) license (https://creativecommons.org/licenses/by/4.0/).

1. Introduction

In recent years, optical perfect absorbers have gained significant attention due to their strong quasi-complete absorption characteristics, integrated capacity, and diverse applications [1]. Researchers are investigating the absorption properties of materials in the THz range to understand their interaction with THz waves. This includes studying the complex refractive index, absorption coefficients, and dielectric properties of different materials. These absorbers are often developed using periodic metamaterials, metasurfaces, or grating structures [2,3]. Metasurfaces have sub-wavelength structures and can conventionally be categorized as 1D and 2D metasurfaces according to their dimensions. Metasurfaces in 1D consist of one-dimensional periodic arrays of subwavelength elements on the surface. A single in-surface-plane direction of variation in the characteristics of 1D metasurfaces provides control over particular aspects of electromagnetic waves, like polarization or phase. Metasurfaces based on gratings, waveguides, or nanowires are examples of 1D metasurfaces [4–6]. Two-dimensional metasurfaces are constructed structures with particular aspects in two dimensions. The subwavelength unit cells are arranged in a planar manner to form a two-dimensional array. It is possible to control the phase, polarization, and amplitude of electromagnetic waves by manipulating the properties of 2D

metasurfaces. Metasurfaces based on arrays of nano-antennas, metasurfaces for beam steering or focusing, and polarization converters are a few examples of 2D metasurfaces [7,8]. Actually, the conventional 1D metasurface is an extension of the 1D gratings, while the conventional 2D metasurface is an extension of the 2D gratings. Here, we expand the metasurface concept to include a vertically structured metasurface (VSM), which consists of a number of sub-wavelength layers of different materials, and along the in-surface-plane directions there is no change in material properties, i.e., no sub-wavelength structures along the in-surface-plane directions. The reason to call such a structure a metasurface is that it has a sub-wavelength structure in the vertical direction and is so thin that it can be considered a surface. Such a VSM is much easier to fabricate than conventional 1D and 2D metasurfaces, so for certain applications, especially absorbers, modulators, filters, and switches, a VSM is much more attractive for production.

There are extensive studies on conventional metasurface absorbers [9] for applications including chemical sensors [9], photoelectric sensors [10], light filters [11], solar energy systems [12], thermal radiators [13,14], multifunctional radar devices [15], integrated devices for seawater detection as well as desalination [16], and harvesting energy and re-radiation devices in solar energy photovoltaic systems [17]. For terahertz applications, the advancements in THz sources, such as quantum cascade lasers, and THz detectors, e.g., bolometers, have improved the efficiency and sensitivity of THz systems. However, challenges remain in developing compact, low-cost, and high-performance THz sources and detectors. Researchers are studying the effects of scattering, absorption, and dispersion, as they are crucial for optimizing THz system performance.

As the VSM absorber is much easier to fabricate than the conventional 1D and 2D metasurface absorbers. In this work, we studied the VSM absorber for terahertz applications. Numerous studies have shown that multilayer, dielectric–metal structures can be used to construct different absorbers [18], e.g., the metal–insulator–metal–insulator–metal (MIMIM) structure [14,15] and the planar bifunctional $HfO_2/Mo/HfO_2$ layered structure [16]. Moreover, structures with graphite [19], liquid crystal [15], VO_2, and $Ge_2Sb_2Te_2$ [20] have been studied to obtain tunable properties with voltage, temperature, and magnetic fields. However, they are not connected to the concept of metasurfaces. According to our extension, such a structure with only a few simple dielectric layers can be viewed as a VSM, and different VSM absorbers can be constructed and studied. On the other hand, investigating new materials and exploring their absorption properties in the THz range can lead to the development of innovative THz devices, such as efficient THz absorbers, filters, and modulators. Therefore, in this study, we investigated a VSM absorber made of insulator–graphene–insulator–graphene–insulator–metal (IGIGIM) layers, aiming at obtaining ultra-wideband strong absorptance in the terahertz region. The insulators used in this study are polymethyl methacrylate (PMMA), SiO_2, and Si, which are basically transparent to terahertz waves.

Ultra-wideband absorbers often face limitations in their performance as the frequency increases. These limitations stem from the difficulties in engineering materials with properties suitable for effective absorption at higher frequencies, leading to suboptimal absorption characteristics. Through proper design of structure and parameter optimization, we obtained broadband absorptance over 80% with a bandwidth of 8.22 THz, from 1.78 to 10.0 THz. Physically, the wide band absorptance of the IGIGIM VSM originates from the multiple Fabry–Pérot-resonance-enhanced absorptions in the structure, which consists of high- and low-refractive index dielectric layers, leading to a number of Fabry–Pérot (FP) micro-resonators in the structure, and the graphene layers and metallic base serve as absorbers. Without the G and M layers, there would be no absorption when ignoring the absorption of other materials, yet without the multiple micro-resonators, the absorption could not be strong and in a wide band. It is the combination of the G and M layers and the micro-resonators that yields the ultra-wide band absorptance.

We utilized the Finite Difference Time Domain (FDTD) method to study the IGIGIM VSM. By varying the thickness of the PMMA layer, we can control the absorption effectiveness across a wide range of working frequencies. Additionally, we investigated

the relationship between the period of the structure and the absorption efficiency. These findings establish a solid theoretical framework for studying terahertz devices based on graphene. And this study is novel because it introduces a new metasurface concept, achieves ultra-wideband and dual broadband absorptance in the THz domain, and demonstrates angle-independent absorptance at a certain range of incidence angles. These findings contribute to the development of efficient and high-quality terahertz wave absorbers with a wide range of applications.

2. Physical Model and Structural Design

The broadband absorber for this purpose is shown in Figure 1. The six-layer insulator–graphene–insulator–graphene–insulator–metal (IGIGIM) material system that we have presented is made up of gold (Au), silicon (Si), graphene (G_1, G_2), silica (SiO_2), and PMMA, as can be seen in the three-dimensional structure in Figure 1a. The Si layer served as the substrate in the six-layer IGIGIM structure. The substrate layer plays a significant role in the overall behavior and performance of the absorber, including its influence on absorption characteristics and resonant modes. The optimum layer thicknesses are h_1 = 0.01 µm, h_2 = 6 µm, h_4 = 9 µm, and h_6 = 14 µm, whereas two-dimensional graphene layers (G_1 and G_2) start from the bottom. We used the 2D graphene layers, and the thickness of a 2D graphene layer is primarily determined by the number of layers stacked. When there is no resonance effect, as the number of graphene layer increases, the absorptance generally increases because one single graphene layer can absorb 2.3% light. However, when the resonance effect is taken into consideration, the absorptance also depends on the quality factor of the resonance as a higher quality factor can lead to stronger confinement of waves, and the waves can be absorbed repeatedly as they go to and fro in the resonator. Due to the resonance effect, even a single layer of graphene can lead to high absorptance. The values along the X and Y axes are $a = b$ = 25 µm. We effectively configured the materials of every layer and modified the thickness of the films to transform them into a perfect absorber, unlike the conventional metal–dielectric stacks built as absorbers.

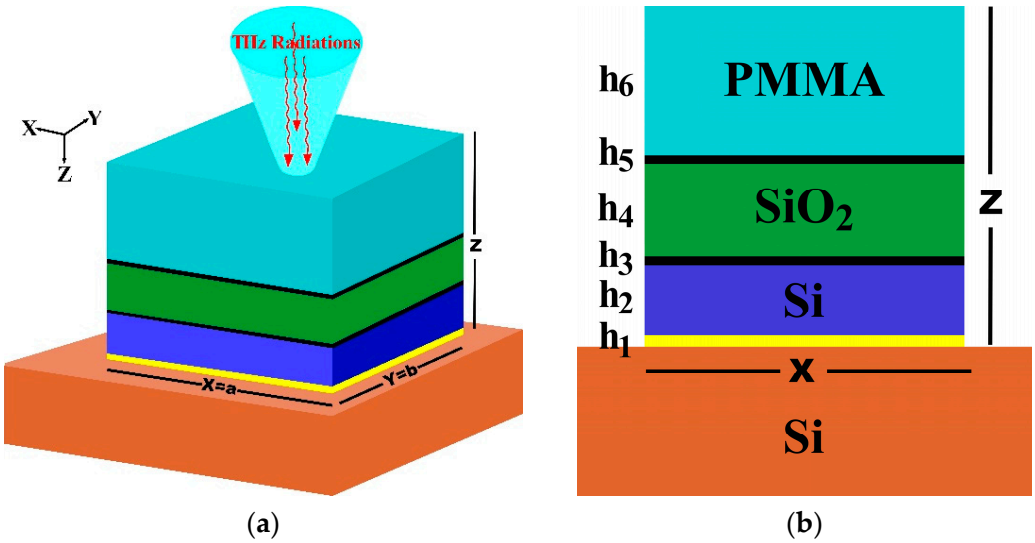

Figure 1. The schematic diagram of a vertically structured IGIGIM metasurface ultra-wideband absorber with different views (**a**) perspective view (**b**) xz view.

In the simulation, the six-layer film structure could be infinitely expanded in both x and y directions, and the planar electromagnetic wave was set to travel along the *z*-axis direction. The periodic boundary conditions were applied to the x- and y-axes, and the maximum and minimum *z*-axis orientations were assigned to a perfectly matched layer (PML) and a perfectly electric conductor (PEC), respectively. The primary goals for developing an ideal absorber are to achieve phase alignment and zero transmission. Thus, $A = 1 - R - T$, where R and T stand for reflectance and transmittance, respectively, can

indicate the absorption rate. Based on the two factors, the absorber can achieve nearly complete absorption when the reflectance and transmittance are minimal or close to zero. In this instance, the rate of absorptance A is the maximum.

Theoretically, the structure can be studied using the one-dimensional transfer matrix method. However, numerical simulation is still required to obtain detailed results from the implicit formulas of reflectivity and transmittivity. As a commercial FDTD tool is available and more powerful, our study used FDTD simulation tools to investigate the optical properties of the proposed structure. Our objective was to demonstrate the optical performance and characteristics of the proposed layered structure through rigorous theoretical analysis and numerical simulations. We employed the FDTD method for thorough simulation and computation of the absorption efficiency of 3D metasurface absorbers using the "Ansys Lumerical 2020 R2.3" Lumerical FDTD solution software. The grid size was chosen to be less than 1/20 of the operating wavelength. We observed the results with a plane wave incident source normal to the structure along the positive z direction. We also discussed the results with different incident angles represented at the end of this section. The frequency domain field and power monitors were used to observe the reflection and transmission, and 1000 frequency points were taken within the used range of THz frequency for smoothness of results. The monitors were placed normal to the z-axes, with the position of the reflection monitor at z_R = 53.4 µm and the transmission monitor at z_T = −35.4 µm, and both monitors were 25 µm × 25 µm in size. The thickness of the Au layer was 0.01 µm. In simulations, we divided the whole surface into small unit cells of side width of 1/8 the shortest wavelength of interest, then in the simulation we simulated the unit cell by using the periodic boundary condition in x- and y-directions, so that the computation time was greatly reduced. The graphene layers together with two small parts from their neighboring layers were treated as an effective layer with an effective refractive index [21], which simplifies the process, allowing for a coarser mesh resolution and reducing computational complexity. The effective refractive index can be calculated using the complex refractive index (CRI) model given by the following Equation (1) [22].

$$n_{Geff} = \frac{V_A n_A + V_B n_B + V_G n_G}{V_A + V_B + V_G} \tag{1}$$

where n_{Geff} is the effective refractive index of the equivalent layer consisting of the graphene layer and the two small pieces with a volume of V_A and V_B taken from the graphene layer's neighboring layers. Note that n_G has an imaginary part, so that it introduces absorption.

The permittivity and refractive index of materials are defined by the refractive index in the software. These parameters are assigned in the simulation by selecting materials in the material database option in the software. The refractive indexes of these materials vary with variation in frequency from 0.1 to 10 THz. Here, we only report the refractive indexes of the materials used at the frequency of 1 THz: the refractive index is 1.14 + 0.78i for PMMA, 2.113 + 2.17i for SiO_2, and 3.42 for Si. The background material set as air has a refractive index of 1.00027; the refractive indices of other materials are derived from data collected by Palik [23]. The Drude–Lorentz model is used to characterize the optical constants of metallic materials such as Au and graphene, as written in Equation (2), and the values of optical constants in eV given in Table 1 [24,25].

$$\varepsilon_m(\omega) = \varepsilon_r - \frac{\omega_{p0}^2}{\omega(\omega + i\gamma_0)} - \frac{\Delta\varepsilon_0 \omega_0^2}{\omega^2 - \omega_0^2 + i\omega\Gamma_0)} \tag{2}$$

where ω is the angular frequency, ω_{p0} is the plasma frequency, γ_0 is the damping coefficient, $\omega\Gamma_0$ is the spectral breadth, and $\Delta\varepsilon_0$ is the weighting factor; these optical constants were used.

Table 1. The optical constants (ε_r, $\Delta\varepsilon_0$, ω_{p0}, γ_0, and Γ_0) of Au and graphene in eV.

Material	ε_r	$\Delta\varepsilon_0$	ω_{p0}	γ_0	Γ_0
Au	5.967	1.09	8.729	0.065	0.433
G	8.5	0.5–0.99	0.64	0.25	0.042

3. Result and Discussion

In FDTD simulations, by examining the power flow and field distributions, we can gain insights into the absorption mechanism and quantify the performance metrics. Figure 2a shows the simulation results from the 3D FDTD approach utilizing the suggested VSM results of the absorber's reflectance {Total (R)}, transmittance {Total (T)}, and absorptance {Total (A)} spectra. Individually, PMMA is a transparent polymer with good mechanical properties. It is commonly used as a protective layer on optical devices. In the absorber, the PMMA layer may protect the underlying layers and provide structural support. The materials PMMA, SiO_2, Si, and Au are arranged in different layers and form a number of FP resonators that cause light of different wavelengths to oscillate strongly in the VSM. Graphene is a two-dimensional material known for its exceptional electrical and optical properties. In this study, the graphene layers (G_1 and G_2) play a role of absorbing THz radiation due to strong light-matter interaction capability. A single layer of graphene can absorb 2.3% of light for a single pass of light through the graphene. However, due to the resonance effect, waves in the structure travel up and down repeatedly, so the light absorption ability of a single layer of graphene can be greatly enhanced. Furthermore, the multiple FP cavities, as shown in Figure 3, have multiple resonance modes; as a result, the absorptance bandwidth can be greatly broadened for proper design of the FP cavities. Au is a highly conductive material with excellent plasmonic properties and also absorbs light. Similar to the case for graphene, due to the multiple FP resonances, the absorption of light by Au is also greatly enhanced in intensity and bandwidth. The Au in the structure also serves as a reflector, preventing light from traveling downward.

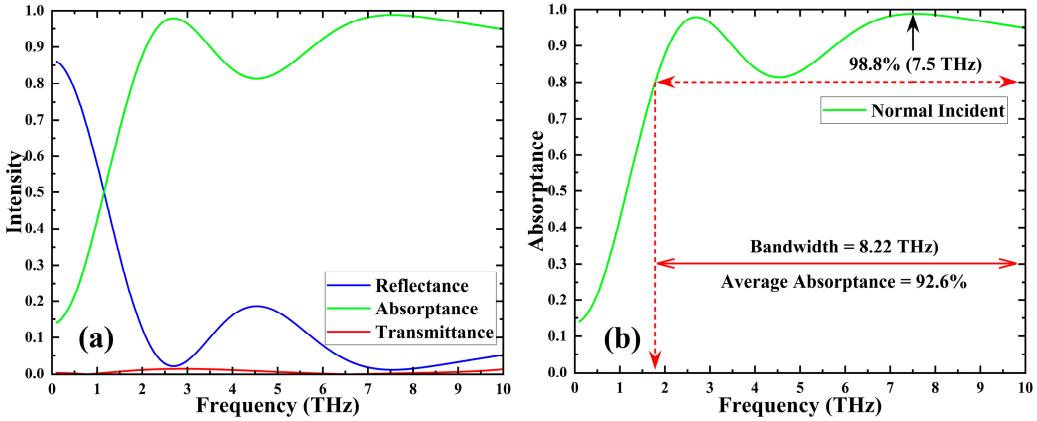

Figure 2. (**a**) Combined spectra of the VSM absorber using the 3D FDTD approach for reflectance (blue line), absorptance (green line), and transmittance (red line). (**b**) Ultra-wideband absorptance spectrum.

By carefully tailoring the parameters of each layer through theoretical analysis and numerical simulations, which are presented in Figures 4–7 and related text, the proposed structure achieves ultra-wideband absorption from 1.78 to 10.0 THz, with a maximum absorption of 98.8% at 7.5 THz. Dual broadband absorptance was obtained for above 90% with the bandwidth of 5.63 THz in the two sub-bands of 2.09–3.5 THz and 5.78–10 THz and above 95% with the bandwidth of 3.63 THz in the two sub-bands of 2.32–3.12 THz and 6.35–9.9 THz. The absorptance of over 80% can be found when the frequency is over 10 THz. However, as we focus our attention to the terahertz frequency region, in this manuscript we omitted the absorption property outside the terahertz frequency region. As

is known, the whole terahertz frequency band is from 0.1 THz to 10 THz. To design an absorber that can cover the entire terahertz frequency band is not practical, i.e., a number of absorbers are needed to cover the whole terahertz frequency band. In this study, we used a high-performance absorber that can cover 82.2% of the whole terahertz frequency band. In a similar way, one can design another absorber to cover the band of the remaining 17.8% of the terahertz frequency band. Therefore, the designed absorber can have wide applications for most terahertz devices. In this work, we focused on the study of improving the optical performance of absorbers by developing a convenient method for creating high-quality absorbers with excellent broadband absorption characteristics.

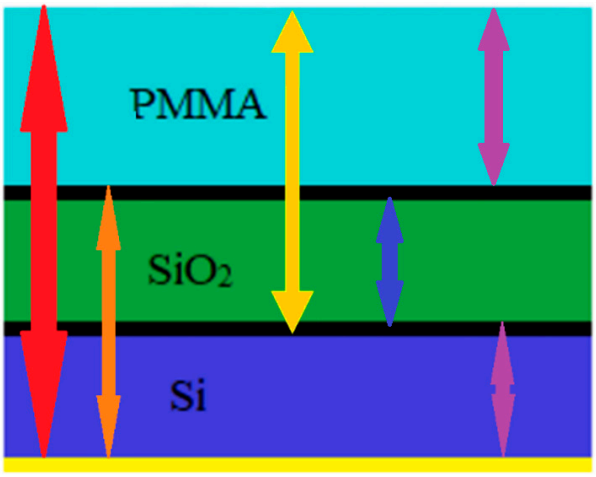

Figure 3. Multiple Fabry–Pérot cavities formed in the structure studied.

The absorber achieves near-zero transmittance while achieving strong absorptance with little reflectance over a broad frequency range from 1.78 to 10.0 THz, as shown in Figure 2b, indicating over 80% absorptance with an average absorptance of 92.6% and a broad absorptance bandwidth of 8.22 THz, making it suitable for ultra-wideband spectroscopy, energy harvesting, sensing, and high signal-to-noise ratio imaging applications, absorbing unwanted signals and enhancing reception capabilities. Additionally, the 7.5 THz peak absorption is up to 98.8%, which can also be utilized in THz spectroscopy to enhance signal-to-noise ratios [26], improve sensitivity [27], and enable precise measurements [28] of THz radiation.

It should be pointed out that in the design, we chose the thicknesses of the PMMA layer at 14 μm, the SiO_2 layer at 9 μm, and the Si layer at 6 μm to make the structures' FP resonance frequencies distribute properly in the terahertz range, so that an ultra-wide absorption band could be obtained. The thickness ranges and their effect on the absorber's performance with different materials are 10–14 μm for PMMA, 7–11 μm for SiO_2, and 2–6 μm for Si, as shown in Figure 4a–c, respectively. The overall absorptance is greater than 80% for all given thicknesses, but the difference is in maximum absorptance, average absorptance, and bandwidth in the given range of operating frequency. Figure 4 shows the influence of thicknesses of PMMA, SiO_2, and Si on the absorptance peaks, which are actually the resonance frequencies of different FP modes.

To analyze the role of the graphene layers, we calculated the case without using the graphene layers, as shown in Figure 5. The presence of graphene layers (G_1 and G_2) within the absorber stack can further enhance absorption due to the unique properties of graphene. Graphene is a two-dimensional material with exceptional conductivity and absorption characteristics across a broad frequency range, including the THz region. The graphene layers serve as thin conductive coatings that can absorb THz radiation, leading to increased overall absorption in the multilayer structure because of resonance [29], as shown in Figure 5. Resonance in the structure enables the graphene to absorb light repeatedly, enabling the thin layer of graphene to absorb light effectively. The physics behind this is that the G and M layers serve as absorbing materials, and there are a number of Fabry–Pérot

(FP) resonators in the structure, as shown in Figure 5. The combination of the G and M layers and the multiple FP resonators leads to the ultra-wideband absorptions. As for the plasmon in the G and M layers, it is natural that plasmons can be excited when these materials are exposed to a light wave, and the plasmons give the nature of absorption for the G and M layers. The effective refractive index of graphene can be modified by controlling the conductivity of the graphene layer. By tuning the chemical potential (Fermi level) of graphene, either through doping or electrostatic gating, the carrier concentration and thus the conductivity of graphene can be controlled.

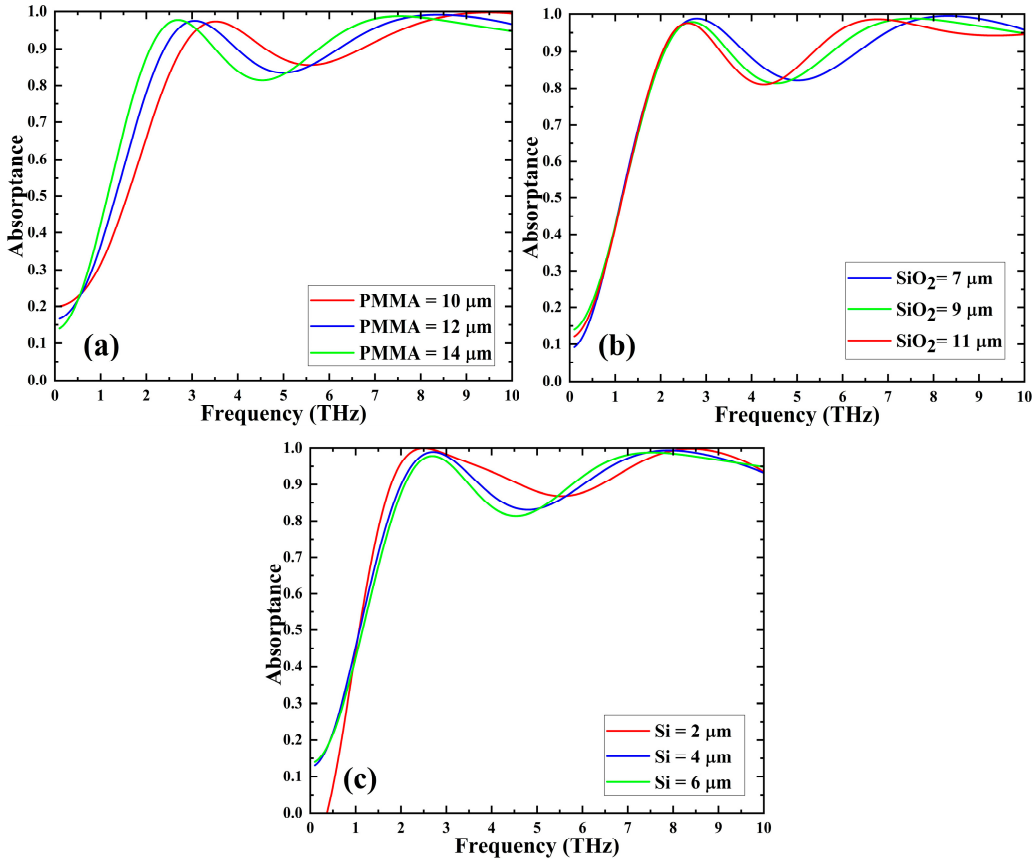

Figure 4. The absorptance curves of stacked layers with different thicknesses used in THz broadband absorbers for (**a**) PMMA for the thickness of SiO_2 = 9 μm and Si = 6 μm, (**b**) SiO_2 for the thickness of PMMA = 14 μm and Si = 6 μm, and (**c**) Si for the thickness of SiO_2 = 9 μm and PMMA = 14 μm.

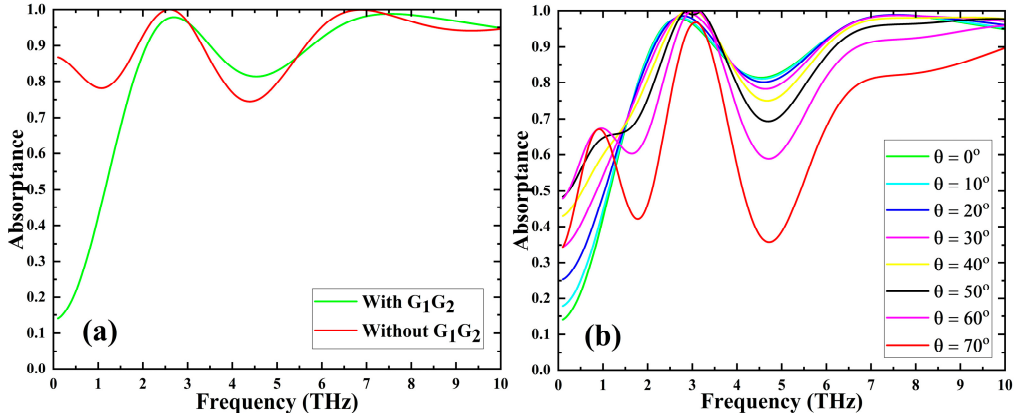

Figure 5. (**a**) The absorptance comparison with and without graphene layers. (**b**) The impact of oblique incident light on performance of the absorber.

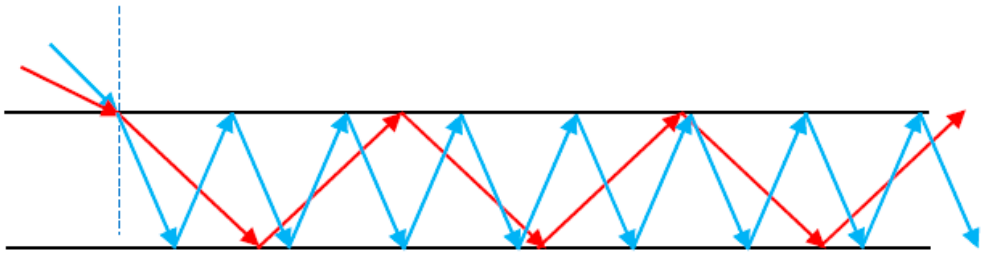

Figure 6. The wave reflection at different incident angles with different reflection times and path length of the wave.

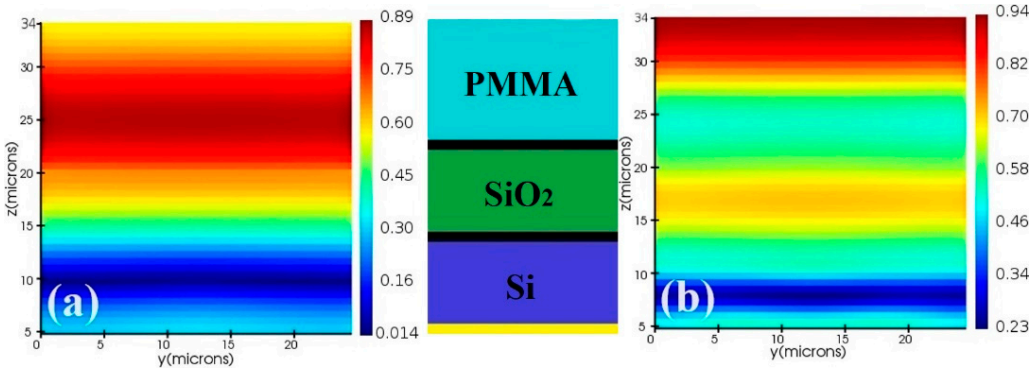

Figure 7. Results of the absorber in the XZ plane (**a**), (**b**) electric field distributions |E| for (**a**) at 4.5 THz and (**b**) at 7.5 THz. The inset serves as a reference of material positions for the field distribution maps.

It should be noted that without the graphene layers, the absorptance property is still acceptable because there are absorptances from the other materials, including PMMA, SiO_2, Si, and Au, in the structure. These materials all have a certain absorptance, and these absorptances are also enhanced by the FP resonances in the structure.

From Figures 4 and 5, we see that there are peaks in the absorptance spectra. Physically, we can understand this by noting that there are Fabry–Pérot (FP) cavities at the interface of each pair of dielectric layers in the layered structure due to reflections of waves at the interface of different materials. As the refractive indexes of PMMA and SiO_2 are approximately the same, the FP resonance effect of these two layers can be neglected, so that we can have two FP cavities in the structure. This explains the two absorptance peaks in Figures 2, 4 and 5 for each group of operating parameters. The Fabry–Pérot cavities, as shown in Figure 3, produce resonances and thus cause resonance absorptions, as indicated by the peaks in the absorptance spectra. From Figure 4a,b, we can see that the absorptance peaks move when the thicknesses of the SiO_2 layer and the PMMA layer change. This is because the cavity length changes accordingly, thus changing the resonance-absorption frequencies. The Fabry–Pérot cavity effect arises from the interference of multiple reflections between parallel reflecting surfaces. In our structure, the interfaces between the layers act as reflecting surfaces, and the differences in refractive indices at these interfaces contribute to the interference patterns. When a THz wave is incident on the structure, it interacts with each layer successively. At each interface between the layers, such as the Au/Si, Si/graphene, graphene/SiO_2, SiO_2/graphene, and graphene/PMMA interfaces, a portion of the incident wave is reflected and transmitted. The reflected waves propagate back and forth between the reflecting surfaces of the structure. At specific frequencies, the reflections constructively interfere, causing FP resonance, leading to enhanced absorption or reflection. The resonance peaks correspond to the frequencies at which constructive interference occurs between the multiple reflections within the Fabry–Pérot cavity. The positions of peaks are influenced by the thicknesses and refractive indices of layers.

In our structure, the refractive index variation in Si, SiO_2, and PMMA with frequency affects the optical path lengths and, consequently, influences the positions of the resonance

peaks. It can be seen from Figure 4 that when the thickness of the dielectric materials increases, the absorption peaks move to the longer wavelength region or lower frequency region. This explains the FP effect mechanism because the increase in dielectric material thickness means longer FP cavities, resulting in a longer resonance wavelength, and thus the absorptance peaks move to the longer wavelength region. It can be seen that the first peak (about 2.75 THz) of absorptance is from the FP resonance absorptance of FP, which is composed of the PMMA (cavity region), and the second peak (about 7.5 THz) is that of FP, which is composed of the whole structure (cavity region).

It is noted further from Figure 5a that the graphene layer can also have a small influence on the absorptance peaks. This is because the graphene has a negative effective dielectric constant, which leads to a smaller effective dielectric constant for the structure, and thus the graphene layer can cause the resonance peaks to slightly move to a higher frequency region because the graphene layer is thin and only has a small influence on the effective refractive index of the structure.

The absorptance comparison of structures with and without graphene layers is also shown in Table 2. By arranging the layers and optimizing their thicknesses, the multilayer stacking THz broadband absorber achieves enhanced absorptance across a wide range of THz frequencies. The selection of PMMA, SiO_2, Si, and graphene, along with the determination of their effective optical thicknesses, enables the absorber to efficiently absorb THz radiation in the specified wavelength regions.

Table 2. The absorptance comparison of the absorber with different conditions.

No.	Structure	Operating Bands	Bandwidth	Average Absorptance
1	Without G_1G_2	5.0–10.0 THz	5.0 THz	94.9%
2	With G_1G_2	1.78–10.0 THz	8.22 THz	92.6%

For a further interest, we assessed the influence of the incident angle of light on the absorptance. As shown in Figure 5b, in the 0.1 to 10 THz frequency range, the average absorptance is over 80% at 0 to 40 degrees because the waves experience more reflection and thus have a longer path and more absorption on the boundaries and inside the layers. However, when the incident angle is over 40 degrees, the absorptance decreases evidently with the incident angle because the reflection times and path lengths decrease evidently at large angles. Other factors such as frequency, polarization, refractive index, and material thickness also influence the absorptance. The structure's combination of absorption and reflection results in high light attenuation, making it an effective absorber. The maximum absorptance of 98.8% at 7.5 THz corresponds to the resonance-absorption frequency, where strong resonance occurs, and the fields are highly confined in the structure and thus leads to the peak absorptance.

Note that the boundaries have limited length along the horizontal axis. This indicates that large-angle incident waves experience shorter reflection times at the absorbing boundaries and shorter paths in the absorbing material between the two boundaries and thus are less absorbed, while small-angle incident waves experience more reflections at the absorbing boundaries (graphene) and longer paths in the absorbing material between the two boundaries and thus are more absorbed, as shown in Figure 6. For simplicity, the reflection over the first horizontal boundary and the refraction at the bottom horizontal boundary are not shown in Figure 6. Furthermore, as the path length and reflection times at the boundaries are mainly decided by the incident angle and size of the structure, a wideband absorptance is possible, as shown in Figure 5b.

To look into the mechanism further, we calculated the electric field distribution in the structure, as shown in Figure 7. From Figure 7a, we can see that the electric field is distributed mainly in the region of the PMMA and SiO_2, confirming the analysis that the resonance peak of 4.5 THz is from the FP resonance formed with these two layers as the resonance region. Also, from Figure 7b, we can see that the electric field is distributed

strongly throughout the whole structure, demonstrating that the resonance absorptance peak of 7.5 THz is from the FP resonator with the whole structure as the resonance region [30,31].

To show the advantages of this work, the previously conducted studies on the multi-layer stacking strategies for broadband absorbers, including their distinctive absorption features, are summarized and compared in Table 3, which shows that the structure studied in this work has the widest absorption bandwidth in the terahertz region of 0.1 THz to 10 THz. It should be pointed out that the structure of G/Topas at line 2 in Table 3 has a greater relative absorptance bandwidth (BWR) of 1.5; however, its bandwidth is only 3.66 THz. Moreover, the structure of Cu/FR-4 at line 3 in Table 3 has a greater absorptance bandwidth of 10.97 GHz; however, its actual bandwidth in the terahertz region of 0.1–10 THz is very small, corresponding to a BWR of only 0.88.

Table 3. Comparison of current results with the literature for various multi-layer stacking designs (average absorption > 80%) and the absorptance performance of broadband absorbers.

Material	Operating Band	BW	*BWR	Ref.
Graphene (G)/Topas	1.45–4.35 THz	2.9 THz	1	[32]
G/Topas	1.12–3.78 THz	3.66 THz	1.5	[33]
Cu/FR-4	3.87–14.84 GHz	10.97 GHz	1.2	[34]
G/Topas/polysilicon/VO_2	1.33–2.83 THz	1.5 THz	0.7	[35]
G/VO_2/Topas/polysilicon	2.05–4.30 THz	2.25 THz	0.7	[36]
Graphite/G/SiO_2	≈7.6–10.5 THz	2.9 THz	0.3	[37]
G/Au/PMMA/SiO_2/Si	1.78–10.0 THz	8.22 THz	1.4	Our Results

*BWR = bandwidth (BW)/central frequency of the absorption band. The bold values are indicating final results of current research.

The above mechanism can be applied to designing ultra-wideband absorbers in other frequency bands, e.g., the mid-infrared band, the near-infrared band, and the visible-light band.

One key characteristic of a perfect absorber is its polarization dependence property. We examined broadband absorptance for s- and p-polarization, as shown in Figure 8. As can be seen From Figure 8, the designed VSM absorber shows polarization-independent absorption spectra. This absorption property of polarization independence can be seen in Figure 6, wherein the reflection times and path length do not depend on the polarization of the incident light to the VSM absorber. Figure 8 further shows that the absorptance for incident angles under 40 degrees is over 80% in the band of 1.78 to 10 THz.

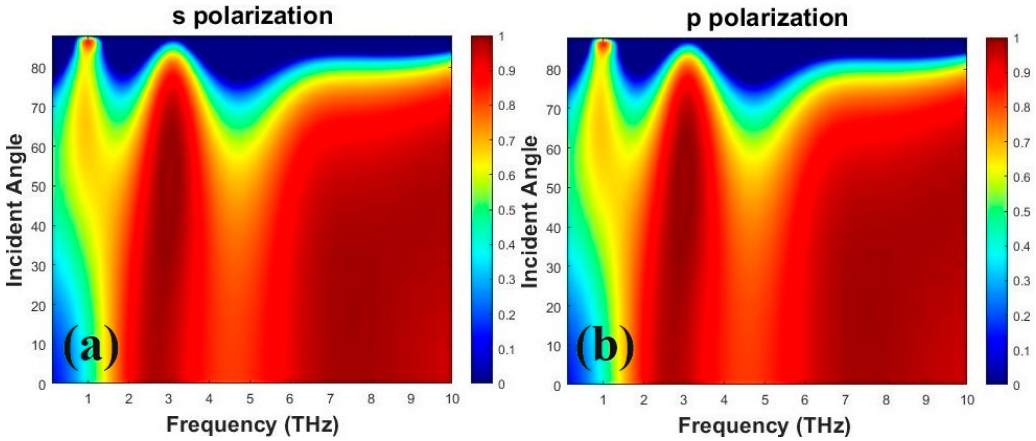

Figure 8. Absorptance spectra for the IGIGIM structure as a function of frequency and angle of incidence for (**a**) s-polarization and (**b**) p-polarization.

Furthermore, the suggested VSM absorber exhibits angle-independent absorptance for both the s- and p-modes at great incident angles, and the absorption spectra are unaltered

for both polarizations at incident angles over 80°. It was determined that the absorber can sustain an average absorptance of 92.6% across wideband 0.1 to 10 THz at the normal incident angle over 80° for both s- and p-polarization.

Although the focus of this paper is simulation research, structural fabrication feasibility still needs to be examined. The following presents a suggested fabrication process that can be used to build the suggested six-layer IGIGIM metasurface absorber's structure for ultra-wideband THz absorption. First, choose a good substrate and clean it thoroughly. Use a deposition method like sputtering to apply a thin coating of Au to the substrate. To specify the required pattern for the gold layer, use lithography. Clean the substrate covered with Au. Use a deposition method such as chemical vapor deposition (CVD) to create a Si layer on top of the Au layer. Use a method like CVD to synthesize high-quality graphene on a metal substrate (such as copper or nickel). Use a transfer technique, such as dry transfer with polymer support, to transfer the produced graphene onto the silicon layer. To ensure optimal adhesion, carefully align the graphene layer on top of the silicon layer. Utilizing a deposition method such as plasma-enhanced chemical vapor deposition (PECVD), deposit a SiO_2 layer on top of the G_1 layer. Create another high-quality graphene layer and use the transfer technique to deposit this synthesized G_2 layer onto the SiO_2 layer. To ensure optimal adhesion, carefully align the graphene layer on top of the silica layer. Deposit a layer of PMMA on top of the graphene layer using spin coating. The PMMA layer can be annealed after deposition to improve stability and adhesion to the graphene layer. After each layer has been deposited, THz spectroscopy can be used to characterize the absorption properties of the newly created THz absorber structure [36,37].

4. Conclusions

In conclusion, this study presents a novel THz wave absorber with a vertically structured, six-layer IGIGIM metasurface capable of achieving ultrawide broadband absorptance in the THz region. By exploring materials with various qualities and optimizing their thickness, the ideal parameters were found. The proposed structure exhibits a broadband absorptance of 81% across the THz range (0.1–10 THz), with a maximum absorptance of 98.8% at 7.5 THz. The structure also demonstrates broadband absorptance from 1.78 to 10.0 THz, with an average absorptance of 92.6% and a bandwidth of 8.22 THz. The multiple FP resonators formed in the structure proposed, together with the graphene and Au layers as absorption materials, provide the mechanism of ultra-wideband absorption in the terahertz region. Additional calculations demonstrate that broadband absorptance has an appropriate tolerance for angles. The mechanism shown can be applied to designing ultra-wideband absorbers in other frequency bands, e.g., the mid-infrared band, the near-infrared band, and the visible-light band. This ideal absorber will open the door to metasurface absorbers, providing new application possibilities for energy-harvesting technologies in solar thermal photovoltaic systems and communication systems.

Author Contributions: Conceptualization, M.A.; methodology, M.A.; software, M.A.; validation, M.A., Q.W. and Z.O.; formal analysis, M.A. and Z.O.; investigation, M.A., Q.W. and Z.O.; resources, Q.W. and Z.O.; data curation, M.A., M.L. and Z.L.; writing—original draft preparation, M.A.; writing—review and editing, M.A., Q.W. and Z.O.; visualization, M.A. and Z.O.; supervision, Z.O.; project administration, M.A., Q.W. and Z.O.; funding acquisition, Q.W. and Z.O. All authors have read and agreed to the published version of the manuscript.

Funding: This work was supported by the Shenzhen Science and Technology Project (JCYJ20190808161801637, JCYJ20180305124247521, JCYJ20190808151017218, 20200812114907001), and Guangdong Province Natural Science Funds (GDNSF) (2020A1515011154).

Data Availability Statement: The data presented in this study are available on request from the corresponding author. The data are not publicly available due to privacy of our project.

Acknowledgments: We thank all authors and contributors for their hard work. We sincerely thank the reviewers and editors.

Conflicts of Interest: The authors declare no conflicts of interest.

References

1. Landy, N.I.; Sajuyigbe, S.; Mock, J.J.; Smith, D.R.; Padilla, W.J. Perfect Metamaterial Absorber. *Phys. Rev. Lett.* **2008**, *100*, 207402. [CrossRef] [PubMed]
2. Gao, H.; Peng, W.; Cui, W.; Chu, S.; Yu, L.; Yang, X. Ultraviolet to near Infrared Titanium Nitride Broadband Plasmonic Absorber. *Opt. Mater.* **2019**, *97*, 109377. [CrossRef]
3. Li, Y.; Liu, Z.; Zhang, H.; Tang, P.; Wu, B.; Liu, G. Ultra-Broadband Perfect Absorber Utilizing Refractory Materials in Metal-Insulator Composite Multilayer Stacks. *Opt. Express* **2019**, *27*, 11809–11818. [CrossRef] [PubMed]
4. Wei, H.; Ge, H.; Zhao, T.; Sharma, S.; Petru, M.; Prakash Dwivedi, S.; Kumar, A.; Abbas, M. Vanadium Dioxide Thin Films-Assisted Terahertz Meta-Surface for Simultaneous Absorption, Polarization Conversion Bi-Functional Switching, and Wavefront Operation. *Results Phys.* **2023**, *53*, 106970. [CrossRef]
5. Edee, K.; Rhouma, M.B.; Fan, J.-A.; Antezza, M.; Gippius, N.; Wang, E.; Plumey, J.-P.; Granet, G.; Guizal, B. Inverse Design of a 1D Dielectric Metasurface by Topology Optimization: Fluctuations-Trend Analysis Assisted by a Diamond-Square Algorithm. *J. Opt. Soc. Am. B* **2020**, *37*, 3721–3728. [CrossRef]
6. Ignatyeva, D.O.; Krichevsky, D.M.; Belotelov, V.I.; Royer, F.; Dash, S.; Levy, M. All-Dielectric Magneto-Photonic Metasurfaces. *J. Appl. Phys.* **2022**, *132*, 100902. [CrossRef]
7. Ullah, Z.; Al Hasanl, M.; Mabrouk, I.B.; Junaid, M.; Sheikh, F. 2D MXene Ti3C2Tx Enhanced Plasmonic Absorption in Metasurface for Terahertz Shielding. *Comput. Mater. Contin.* **2023**, *75*, 3453–3464. [CrossRef]
8. Yildirim, D.U.; Ghobadi, A.; Soydan, M.C.; Serebryannikov, A.E.; Ozbay, E. One-Way and near-Absolute Polarization Insensitive near-Perfect Absorption by Using an All-Dielectric Metasurface. *Opt. Lett.* **2020**, *45*, 2010–2013. [CrossRef]
9. De Marcellis, A.; Palange, E.; Janneh, M.; Rizza, C.; Ciattoni, A.; Mengali, S. Design Optimisation of Plasmonic Metasurfaces for Mid-Infrared High-Sensitivity Chemical Sensing. *Plasmonics* **2017**, *12*, 293–298. [CrossRef]
10. Kazanskiy, N.L.; Khonina, S.N.; Butt, M.A. Recent Development in Metasurfaces: A Focus on Sensing Applications. *Nanomaterials* **2023**, *13*, 118. [CrossRef]
11. Zhu, W.; Guo, L.; Du, K.; Zhang, B.; Zhou, C.; Chen, G.; Bai, J.; Xu, M.; Wang, S. Continuously Controlling the Phase Transition of In3SbTe2 for Tunable High Quality-Factors Absorber. *Opt. Laser Technol.* **2023**, *162*, 109239. [CrossRef]
12. Su, W.; Ding, Z.; Luo, Y.; Ye, L.; Wu, H.; Yao, H. Machine Learning-Enabled Design of Metasurface Based near-Perfect Daytime Radiative Cooler. *Sol. Energy Mater. Sol. Cells* **2023**, *260*, 112488. [CrossRef]
13. Sreekanth, K.V.; Sreejith, S.; Han, S.; Mishra, A.; Chen, X.; Sun, H.; Lim, C.T.; Singh, R. Biosensing with the Singular Phase of an Ultrathin Metal-Dielectric Nanophotonic Cavity. *Nat. Commun.* **2018**, *9*, 369. [CrossRef] [PubMed]
14. Zhou, W.-X.; Shen, Y.; Hu, E.-T.; Zhao, Y.; Sheng, M.-Y.; Zheng, Y.-X.; Wang, S.-Y.; Lee, Y.-P.; Wang, C.-Z.; Lynch, D.W.; et al. Nano-Cr-Film-Based Solar Selective Absorber with High Photo-Thermal Conversion Efficiency and Good Thermal Stability. *Opt. Express* **2012**, *20*, 28953–28962. [CrossRef] [PubMed]
15. Zhou, S.; Shen, Z.; Kang, R.; Ge, S.; Hu, W. Liquid Crystal Tunable Dielectric Metamaterial Absorber in the Terahertz Range. *Appl. Sci.* **2018**, *8*, 2211. [CrossRef]
16. Chen, C.; Zhou, L.; Yu, J.; Wang, Y.; Nie, S.; Zhu, S.; Zhu, J. Dual Functional Asymmetric Plasmonic Structures for Solar Water Purification and Pollution Detection. *Nano Energy* **2018**, *51*, 451–456. [CrossRef]
17. Wang, H.; Chang, J.Y.; Yang, Y.; Wang, L. Performance Analysis of Solar Thermophotovoltaic Conversion Enhanced by Selective Metamaterial Absorbers and Emitters. *Int. J. Heat Mass Transf.* **2016**, *98*, 788–798. [CrossRef]
18. Chaudhuri, K.; Alhabeb, M.; Wang, Z.; Shalaev, V.M.; Gogotsi, Y.; Boltasseva, A. Highly Broadband Absorber Using Plasmonic Titanium Carbide (MXene). *ACS Photonics* **2018**, *5*, 1115–1122. [CrossRef]
19. Wang, H.; Yang, Y.; Wang, L. Switchable Wavelength-Selective and Diffuse Metamaterial Absorber/Emitter with a Phase Transition Spacer Layer. *Appl. Phys. Lett.* **2014**, *105*, 071907. [CrossRef]
20. Guo, Y.; Zhang, Y.; Chai, X.; Zhang, L.; Wu, L.; Cao, Y.; Song, L. Tunable Broadband, Wide Angle and Lithography-Free Absorber in the near-Infrared Using an Ultrathin VO_2 Film. *Appl. Phys. Express* **2019**, *12*, 071005. [CrossRef]
21. Liu, W.; Liu, H.; Sun, X.; Zhang, F. The Design of Large Curved Waveguide Based on Sunflower Graded Photonic Crystal. *Photonics* **2023**, *10*, 781. [CrossRef]
22. Li, Y.; Zhang, Z.; Zhang, T.; Zhao, X.; Yu, Y.; Li, X.; Wu, X. Quantitative Analysis of Iron Rust Using Terahertz Time-Domain Spectroscopy. *J. Nondestruct. Eval.* **2023**, *42*, 7. [CrossRef]
23. Palik, E.D. *Handbook of Optical Constants of Solids*; Academic Press: Cambridge, MA, USA, 1998; Volume 3, ISBN 0125444230.
24. Rodrigo, S.G.; García-Vidal, F.J.; Martín-Moreno, L. Influence of Material Properties on Extraordinary Optical Transmission through Hole Arrays. *Phys. Rev. B* **2008**, *77*, 075401. [CrossRef]
25. Ugawa, A.; Rinzler, A.G.; Tanner, D.B. Far-Infrared Gaps in Single-Wall Carbon Nanotubes. *Phys. Rev. B.* **1999**, *60*, R11305. [CrossRef]
26. Pai, A.R.; Lu, Y.; Joseph, S.; Santhosh, N.M.; Degl'Innocenti, R.; Lin, H.; Letizia, R.; Paoloni, C.; Thomas, S. Ultra-Broadband Shielding of Cellulose Nanofiber Commingled Biocarbon Functional Constructs: A Paradigm Shift towards Sustainable Terahertz Absorbers. *Chem. Eng. J.* **2023**, *467*, 143213. [CrossRef]

27. Wang, D.; Xu, K.D.; Luo, S.; Cui, Y.; Zhang, L.; Cui, J. A High Q-Factor Dual-Band Terahertz Metamaterial Absorber and Its Sensing Characteristics. *Nanoscale* **2023**, *15*, 3398–3407. [CrossRef]
28. Alsalman, O.; Wekalao, J.; Arun Kumar, U.; Agravat, D.; Parmar, J.; Patel, S.K. Design of Split Ring Resonator Graphene Metasurface Sensor for Efficient Detection of Brain Tumor. *Plasmonics* **2023**. [CrossRef]
29. Danish, M.; Raza, M.T.; Iftikhar, M.; Hassan, I.; Husnain, S.A.; ul Hassan, M.M.; Mumtaz, M.; Khan, A.M.; Noor, H.; Shahazad, F. Spray Deposited Graphene@MXene on a Flexible Polymer Substrate for Terahertz Shielding. *Mater. Chem. Phys.* **2023**, *311*, 128573. [CrossRef]
30. Liu, W.; Song, Z.; Wang, W. A High-Performance Broadband Terahertz Absorber Based on Multilayer Graphene Squares. *Phys. Scr.* **2021**, *96*, 055504. [CrossRef]
31. Ghosh, S.; Bhattacharyya, S.; Chaurasiya, D.; Srivastava, K.V. An Ultrawideband Ultrathin Metamaterial Absorber Based on Circular Split Rings. *IEEE Antennas Wirel. Propag. Lett.* **2015**, *14*, 1172–1175. [CrossRef]
32. Lim, D.; Lim, S. Ultrawideband Electromagnetic Absorber Using Sandwiched Broadband Metasurfaces. *IEEE Antennas Wirel. Propag. Lett.* **2019**, *18*, 1887–1891. [CrossRef]
33. Ye, L.; Chen, X.; Zhu, C.; Li, W.; Zhang, Y. Switchable Broadband Terahertz Spatial Modulators Based on Patterned Graphene and Vanadium Dioxide. *Opt. Express* **2020**, *28*, 33948–33958. [CrossRef] [PubMed]
34. Liu, Y.; Huang, R.; Ouyang, Z. Terahertz Absorber with Dynamically Switchable Dual-Broadband Based on a Hybrid Metamaterial with Vanadium Dioxide and Graphene. *Opt. Express* **2021**, *29*, 20839–20850. [CrossRef] [PubMed]
35. Varshney, G.; Rani, N.; Pandey, V.S.; Yaduvanshi, R.S.; Singh, D. Graphite/Graphene Disk Stack-Based Metal-Free Wideband Terahertz Absorber. *J. Opt. Soc. Am. B* **2021**, *38*, 530–538. [CrossRef]
36. El-Hageen, H.M.; Sorathiya, V.; Lavadiya, S.; Mehata, N.; Katariya, V.; Patel, S.K.; Albalawi, H.; Alatwi, A.M.; Alhartomi, M.A.; Mead, M.A.; et al. Multilayered Gold, MgF2 and Tungsten Based Ultra Wide Band Infrared Absorber for Solar Cell Applications. *Mater. Chem. Phys.* **2023**, *301*, 127680. [CrossRef]
37. Zhou, Y.; Qin, Z.; Liang, Z.; Meng, D.; Xu, H.; Smith, D.R.; Liu, Y. Ultra-Broadband Metamaterial Absorbers from Long to Very Long Infrared Regime. *Light Sci. Appl.* **2021**, *10*, 138. [CrossRef]

Disclaimer/Publisher's Note: The statements, opinions and data contained in all publications are solely those of the individual author(s) and contributor(s) and not of MDPI and/or the editor(s). MDPI and/or the editor(s) disclaim responsibility for any injury to people or property resulting from any ideas, methods, instructions or products referred to in the content.